Electronic Supplementary Information

Bioinspired Sea-sponge Nanostructure Design of Ni/Ni(HCO$_3$)$_2$-on-C for Supercapacitor with Superior Anti-fading Capacity

Qingnan Wu, Jiahao Wen, Ming Wen, Qingsheng Wu, and Yongqing Fu*

Experimental section

1. Chemicals

The reagents used in this study include: sodium chloroacetate (ClCH$_2$COONa, Aladdin Chemistry Co., Ltd, ≥98%), nickel nitrate hexahydrate (Ni(NO$_3$)$_2$·6H$_2$O, Aladdin Chemistry Co., Ltd, ≥98%), sodium bicarbonate (NaHCO$_3$, Aladdin Chemistry Co., Ltd, ≥99.8%), urea (H$_2$NCONH$_2$, Sinopharm Chemical Reagent Co., Ltd, ≥99%), ethylene glycol (C$_2$H$_6$O$_2$, Sinopharm Chemical Reagent Co., Ltd, ≥99.0%), ethanol (C$_2$H$_6$O, Sinopharm Chemical Reagent Co., Ltd, ≥99.7%). All the reagents were analytical purity and used without further purification.

2. Synthesis of *S*-PCSs

The *S*-PCSs were prepared using a spray pyrolysis method. The sodium chloroacetate (19.97 g) was dispersed into the deionized water (100 mL) under a constant magnetic stirring for 30 min. The obtained solution was put into a humidifier. When the temperature of the tube furnace reached to 700℃, the steams were blow with the carrier gas (Ar) to complete the process of thermal decomposition. Finally, the product was collected, washed by a solution of ethanol and deionized water (volume ratio of 3:1 between them), and finally dried at 60℃ in a vacuum chamber overnight for further use.

3. Preparation of working electrodes

A mixture of Ni/Ni(HCO$_3$)$_2$-on-C (80 wt%), acetylene black (10 wt%) and poly (tetrafluoroethylene) (10 wt%) was ground with ethanol to form a homogeneous slurry, which was spread on the nickel foam and subsequently pressed under 8 MPa. Then, the formed working electrode was dried at 100℃ in a vacuum oven overnight. The final mass of active materials was weighed. The *S*-PCSs working electrodes were also prepared in the same way by replacing Ni/Ni(HCO$_3$)$_2$-on-C with *S*-PCSs.

4. Electrochemical measurement

Cyclic voltammetry (CV) and galvanostatic charging-discharging (GCD) of as-treated Ni/Ni(HCO$_3$)$_2$-on-C were measured in a KOH (6 M) aqueous electrolyte using a CHI660E electrochemical work station (Chenhua, Shanghai, China) with a three-electrode configuration. The platinum plate and saturated calomel electrodes (SCE) were used as counter and reference electrodes, respectively. The Ni/Ni(HCO$_3$)$_2$-on-C//*S*-PCSs asymmetric supercapacitor was fabricated. A cellulose paper was used as the separator and 6 M KOH was used as the electrolyte.
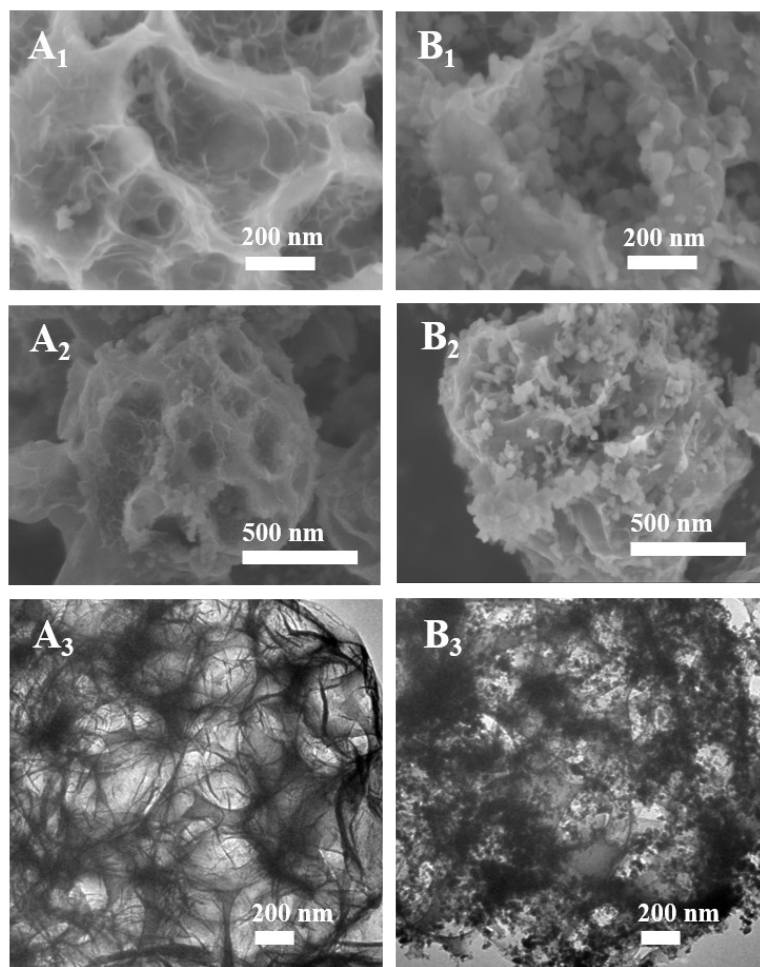
Fig. S1. The SEM and TEM images of obtained Ni(HCO$_3$)$_2$-on-C samples under different stages: (A) 0.5 mmol Ni(NO$_3$)$_2$·6H$_2$O and 2 mmol urea in 12 mL mixed solution; (B) 1 mmol Ni(NO$_3$)$_2$·6H$_2$O and 4 mmol urea in 12 mL mixed solution.
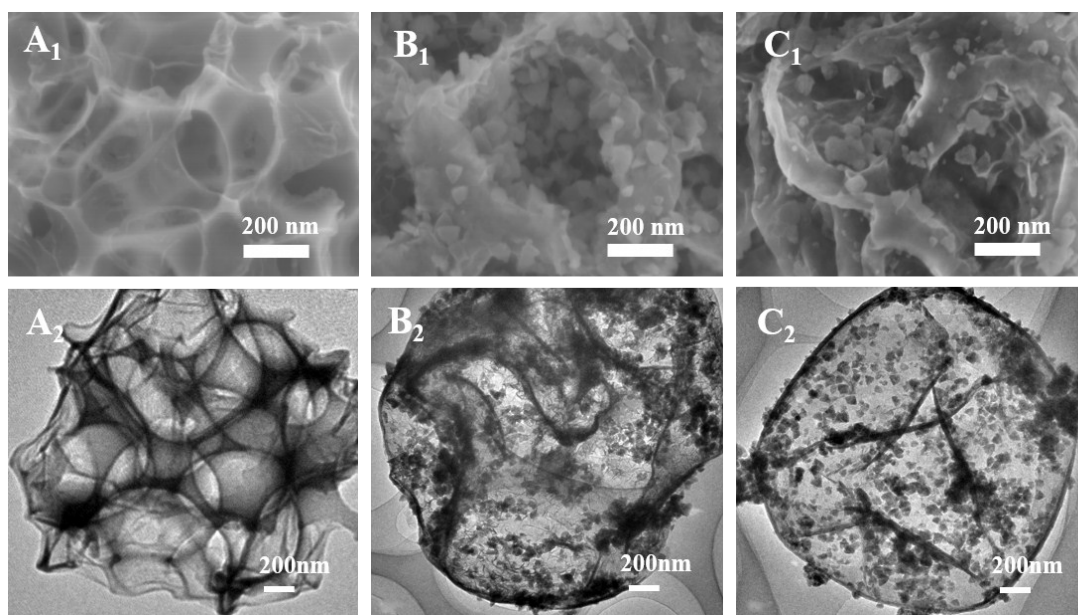
Fig. S2. The high magnification SEM and TEM images of (A) *S*-PCSs, (B) Ni(HCO$_3$)$_2$-on-C and (C) Ni/Ni(HCO$_3$)$_2$-on-C.
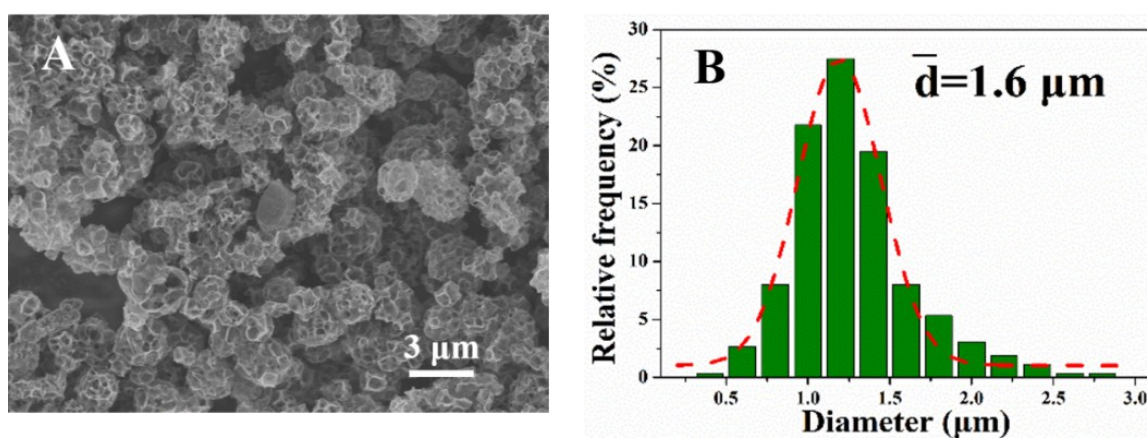

Fig. S3. (A) The low magnification SEM images of *S*-PCSs and (B) its corresponding distribution column diagram.

Table S1. BET data of *S*-PCSs, Ni(HCO$_3$)$_2$-on-C and Ni/Ni(HCO$_3$)$_2$-on-C.

Sample	*S*-PCSs	Ni(HCO$_3$)$_2$-on-C	Ni/Ni(HCO$_3$)$_2$-on-C
BET surface areas (m^2 g^{-1})	213.3640	125.2596	93.4381
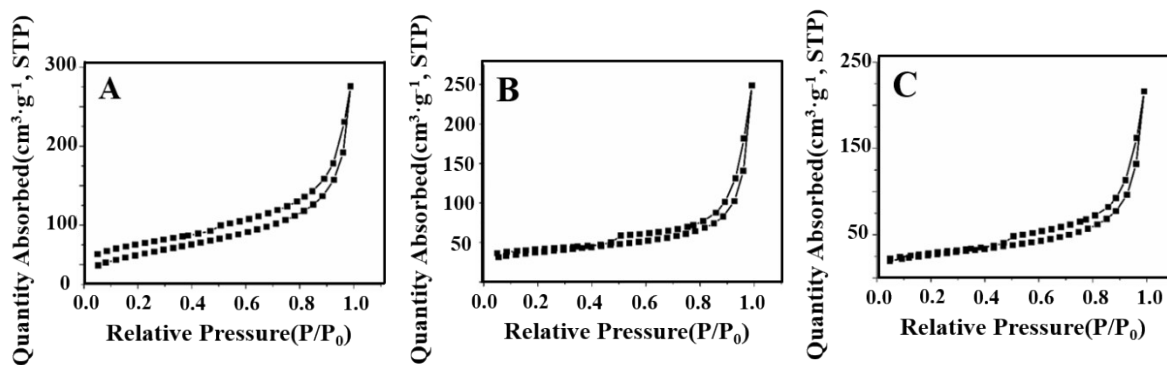
Fig. S4. The nitrogen adsorption-desorption isotherms of (A) *S*-PCSs, (B) Ni(HCO$_3$)$_2$-on-C and (C) Ni/Ni(HCO$_3$)$_2$-on-C.
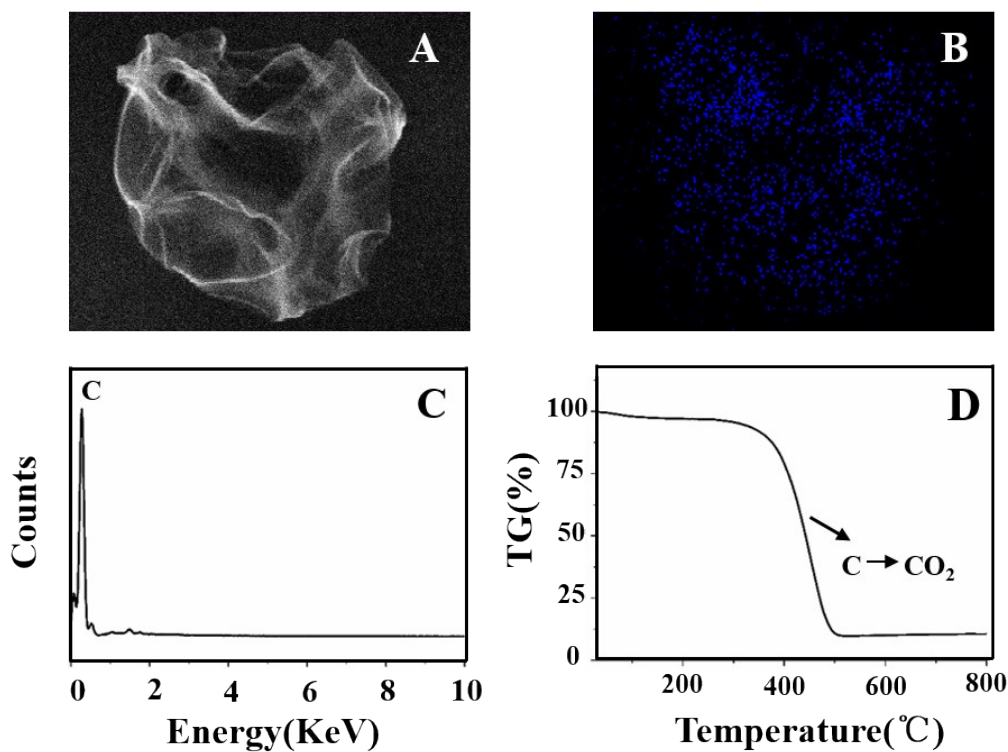
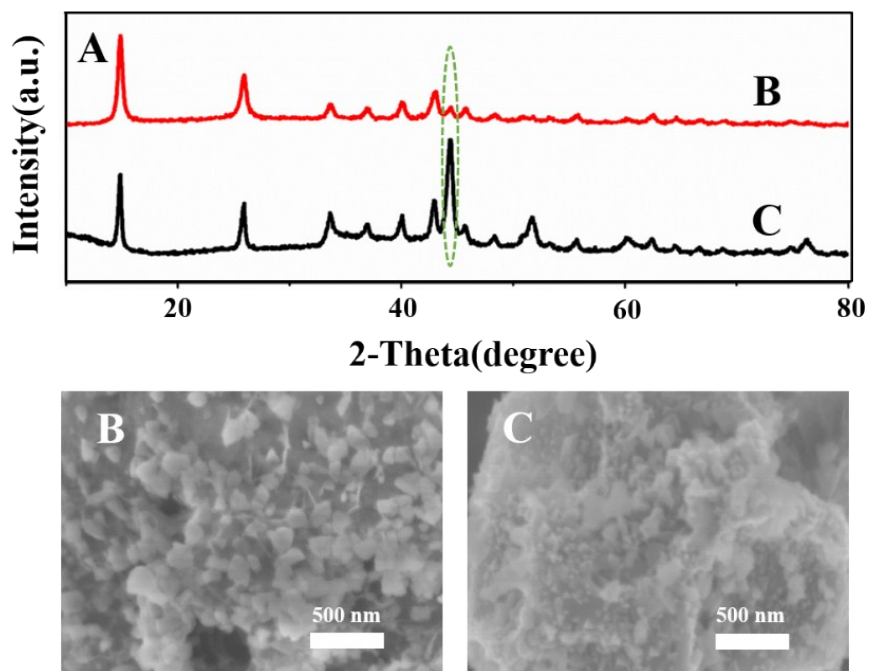**Fig. S5.** (A&B) The EDX mapping analysis, (C) EDX and (D) TG patterns of *S*-PCSs.

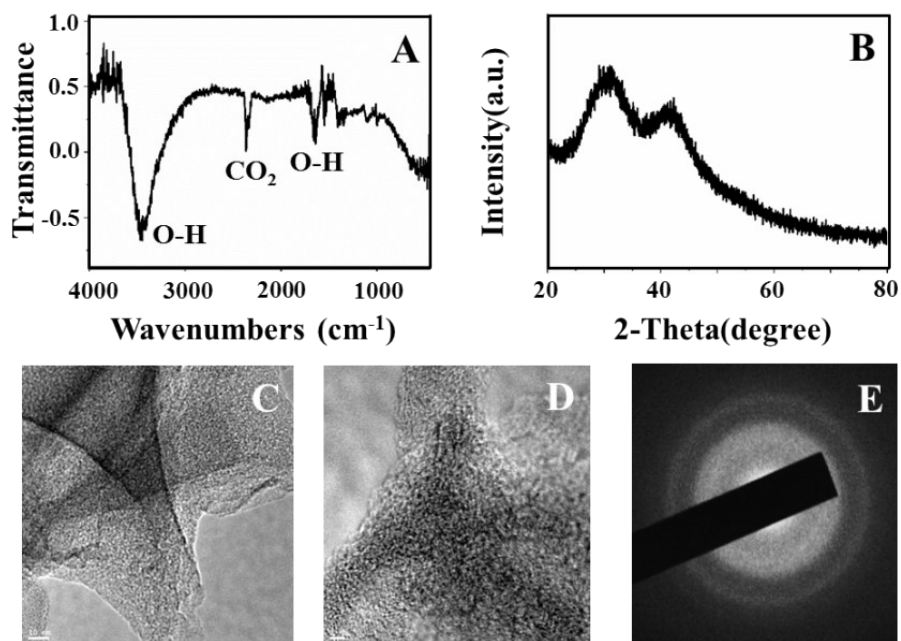**Fig. S6** (A) The XRD patterns and (B, C) SEM images of different Ni contents.

Fig. S7 The property characterizations of *S*-PCSs: (A) FT-IR; (B) XRD pattern; (C, D) the high magnification TEM images; (E) SAED pattern.
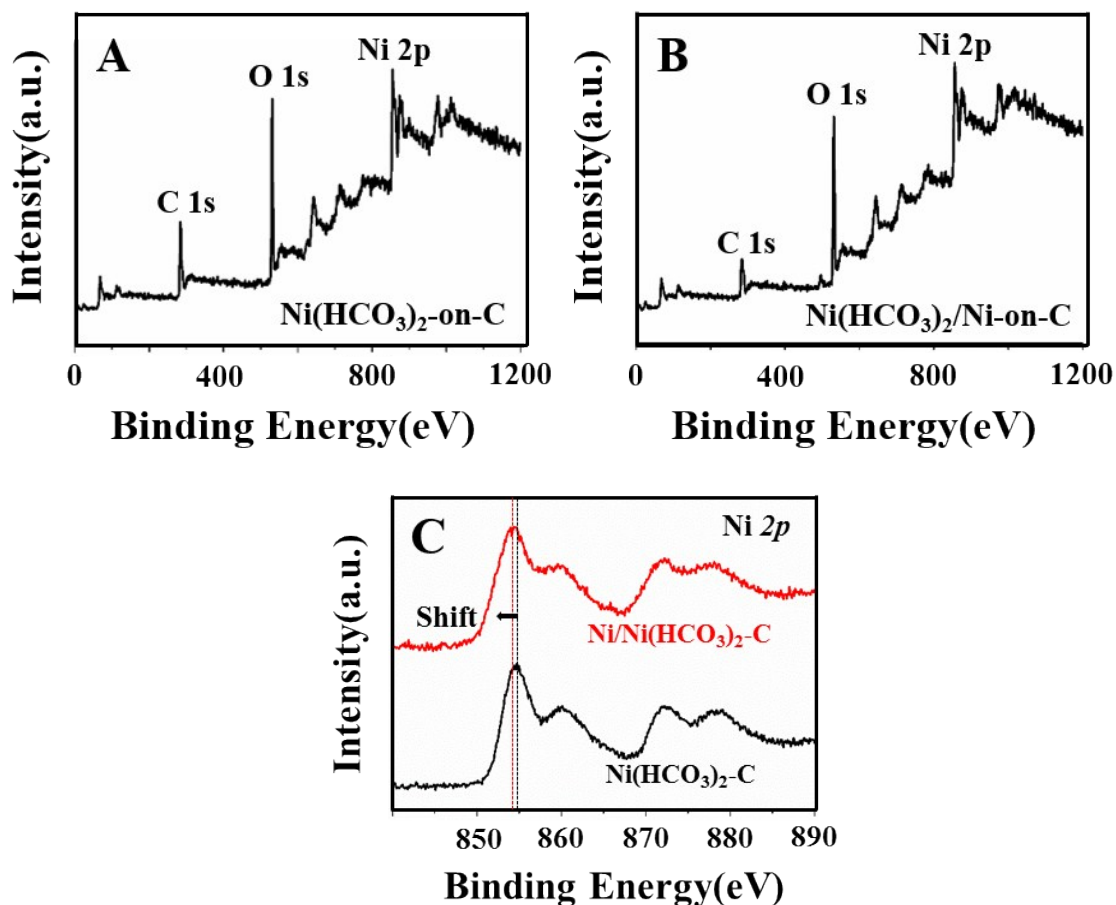
5

Fig. S8 The survey spectra of (A) Ni(HCO$_3$)$_2$-on-C and (B) Ni/Ni(HCO$_3$)$_2$-on-C. (C) The comparision of raw data Ni *2p* XPS spectra of Ni/Ni(HCO$_3$)$_2$-on-C and Ni(HCO$_3$)$_2$-on-C.
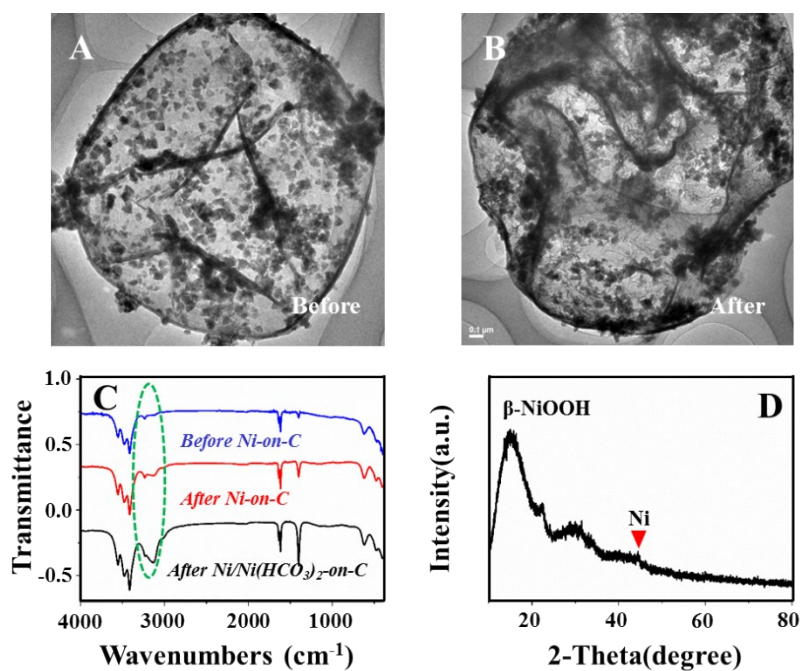

Fig. S9. (A, B) TEM images of Ni/Ni(HCO$_3$)$_2$-on-C before and after activation. (C) FT-IR patterns of Ni-on-C before activation (blue), Ni-on-C (red) and Ni/Ni(HCO$_3$)$_2$-on-C (black) after activation. (D) XRD pattern of Ni/Ni(HCO$_3$)$_2$-on-C after activation.
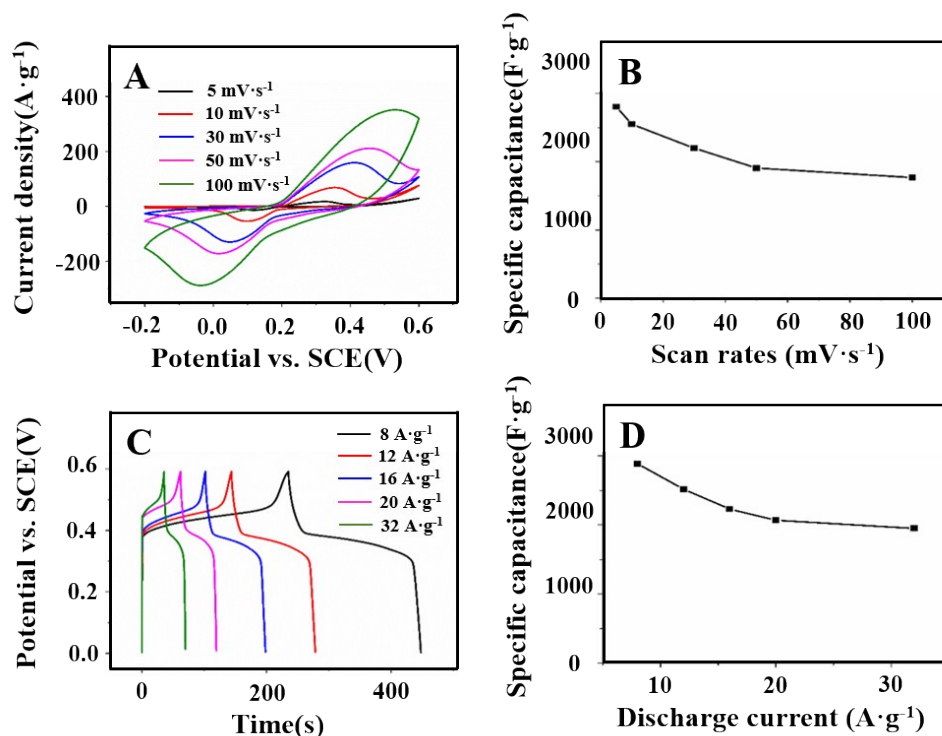
6

Fig. S10. Electrochemical characterizations of Ni/Ni(HCO$_3$)$_2$-on-C: (A) CV curves at various scan rates. (B) The specific capacitances at different scan rates calculated by CV curves. (C) GCD curves at the different current densities. (D) The specific capacitances at different current densities calculated by discharging curves.
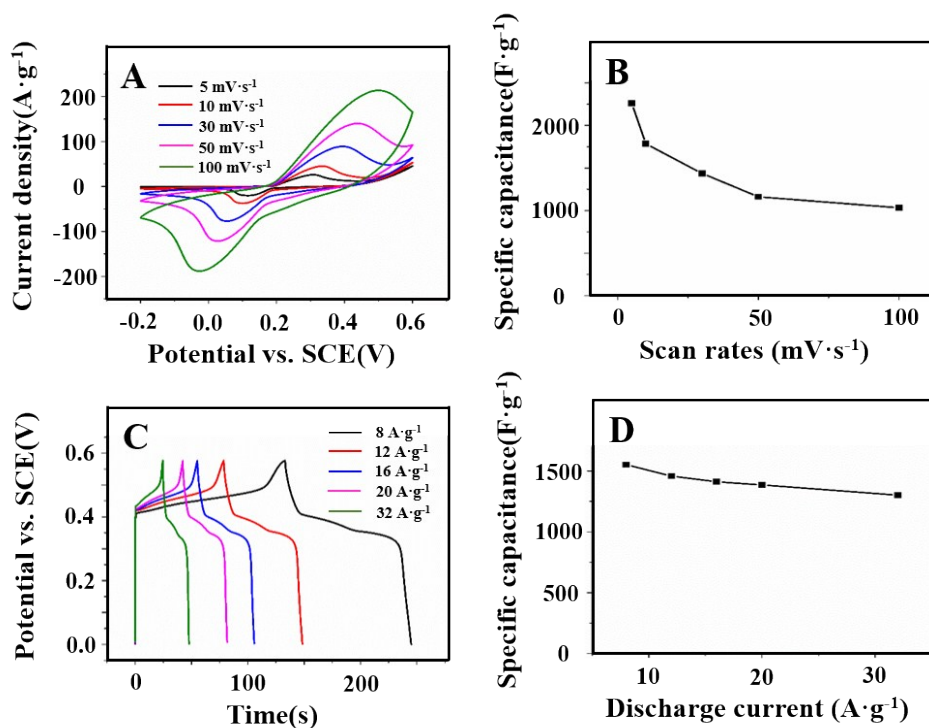

Fig. S11. Electrochemical characterizations of Ni(HCO$_3$)$_2$-on-C: (A) CV curves at various scan rates. (B) The specific capacitances at different scan rates calculated by CV curves. (C) GCD curves at the different current densities. (D) The specific capacitances at different current densities calculated by discharging curves.
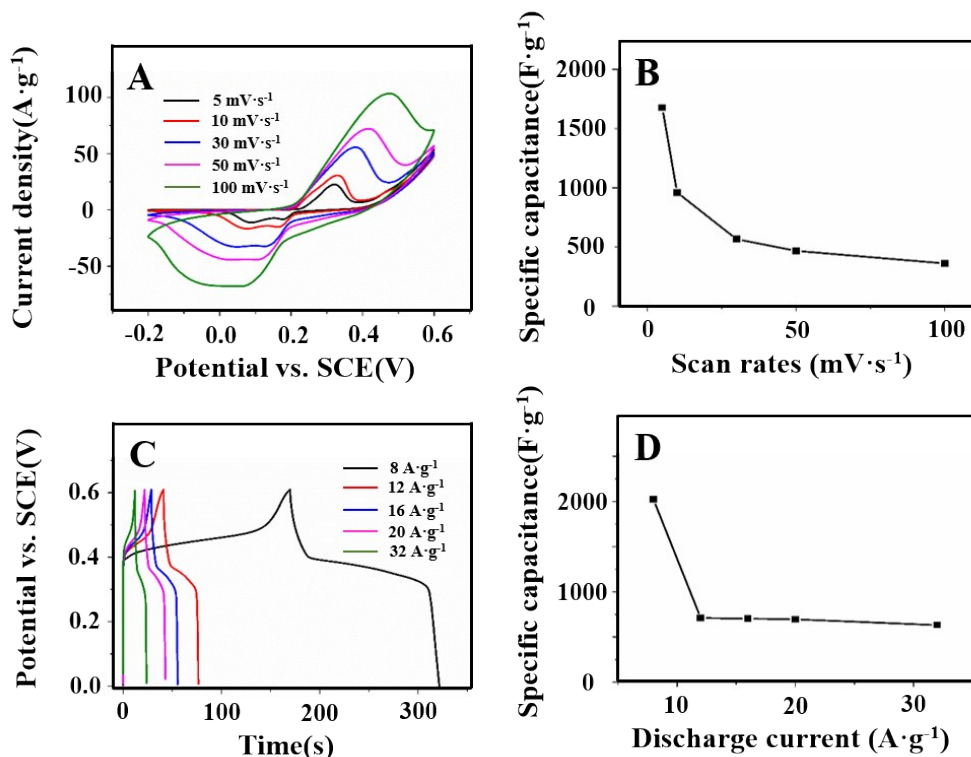
Fig. S12. Electrochemical characterizations of Ni(HCO$_3$)$_2$: (A) CV curves at various scan rates. (B) The specific capacitances at different scan rates calculated by CV curves. (C) GCD curves at the different current densities. (D) The specific capacitances at different current densities calculated by discharging curves.
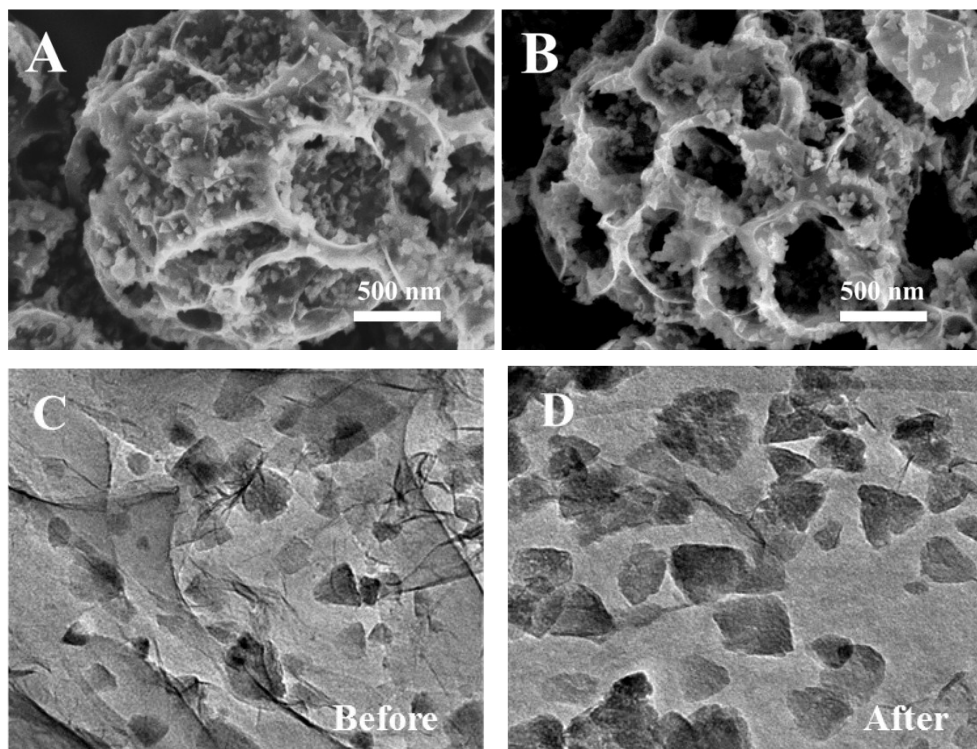

Fig. S13. SEM and TEM images of Ni/Ni(HCO$_3$)$_2$-on-C before and after cycle life: (A)&(C) Before and (B)&(D) After.
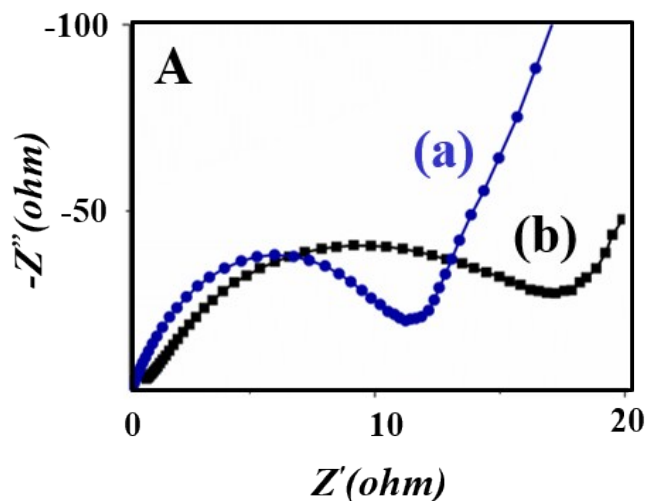
Fig. S14. The Nyquist plots of *S*-PCSs and Ni/Ni(HCO$_3$)$_2$-on-C.
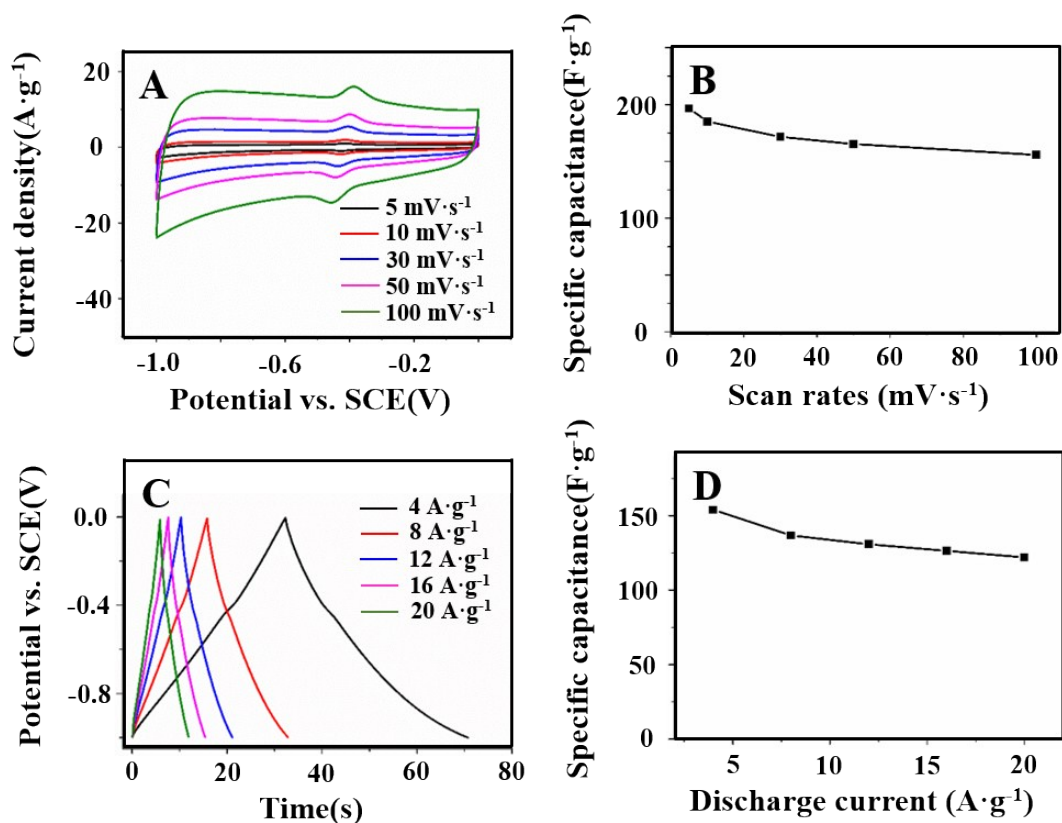

Fig. S15. Electrochemical characterizations of *S*-PCSs: (A) CV curves at various scan rates. (B) The specific capacitances at different scan rates calculated by CV curves. (C) GCD curves at the different current densities. (D) The specific capacitances at different current densities calculated by discharging curves.
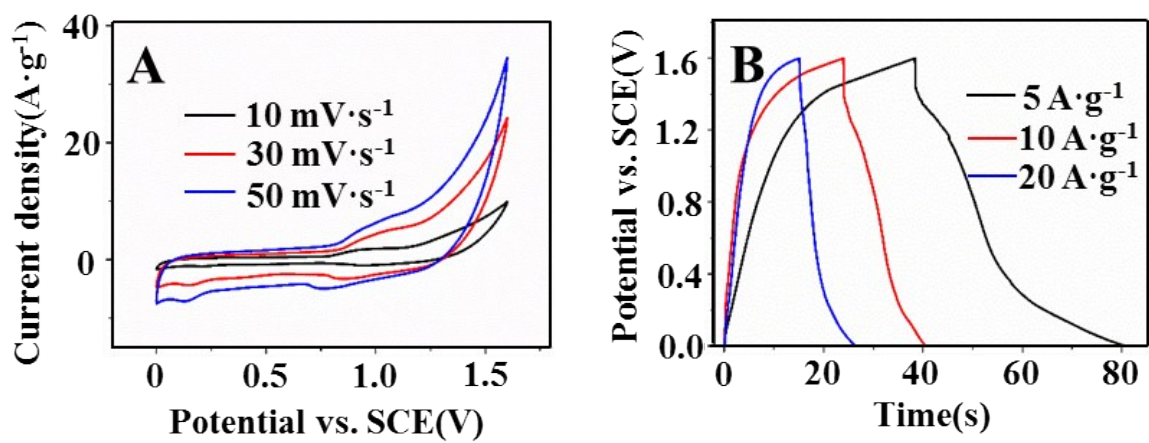
Fig. S16. Electrochemical characteristics of Ni/Ni(HCO$_3$)$_2$-on-C//*S*-PCSs. (A) CV curves at different scan rates. (B) GCD curves at different current densities.